frontiers | Frontiers in Immunology

TYPE Original Research
PUBLISHED 27 October 2023
DOI 10.3389/fimmu.2023.1282653

OPEN ACCESS

EDITED BY
Soren Skov,
University of Copenhagen, Denmark

REVIEWED BY
Fanrong Liu,
Second Affiliated Hospital of Nanchang University, China
Paola Trono,
National Research Council (CNR), Italy

*CORRESPONDENCE
Dipankar Nandi
nandi@iisc.ac.in

RECEIVED 24 August 2023
ACCEPTED 17 October 2023
PUBLISHED 27 October 2023

CITATION
Chattopadhyay A, Jagdish S, Karhale AK, Ramteke NS, Zaib A and Nandi D (2023) IFN-γ lowers tumor growth by increasing glycolysis and lactate production in a nitric oxide-dependent manner: implications for cancer immunotherapy.
Front. Immunol. 14:1282653.
doi: 10.3389/fimmu.2023.1282653

IFN-γ lowers tumor growth by increasing glycolysis and lactate production in a nitric oxide-dependent manner: implications for cancer immunotherapy

Avik Chattopadhyay, Sirisha Jagdish, Aagosh Kishor Karhale, Nikita S. Ramteke, Arsha Zaib and Dipankar Nandi*

Department of Biochemistry, Indian Institute of Science, Bangalore, India

Introduction: Interferon-gamma (IFN-γ), the sole member of the type-II interferon family, is well known to protect the host from infectious diseases as well as mount anti-tumor responses. The amounts of IFN-γ in the tumor microenvironment determine the host responses against tumors; however, several tumors employ evasive strategies by responding to low IFN-γ signaling.

Methods: In this study, the response of various tumor cell lines to IFN-γ was studied *in vitro*.

Results: IFN-γ-activation increases glycolytic flux and reduces mitochondrial function in a nitric oxide (NO)- and reactive oxygen species (ROS)-dependent manner in the H6 hepatoma tumor cell line. The higher glycolysis further fueled NO and ROS production, indicating a reciprocal regulation. These processes are accompanied by Hypoxia inducing factor (HIF)-1α stabilization and HIF-1α-dependent augmentation of the glycolytic flux. The IFN-γ enhancement of lactate production also occurred in other NO-producing cell lines: RAW 264.7 monocyte/macrophage and Renca renal adenocarcinoma. However, two other tumor cell lines, CT26 colon carcinoma and B16F10 melanoma, did not produce NO and lactate upon IFN-γ-activation. HIF-1α stabilization upon IFN-γ-activation led to lower cell growth of B16F10 but not CT26 cells. Importantly, the IFN-γ-activation of both CT26 and B16F10 cells demonstrated significant cellular growth reduction upon metabolic rewiring by exogenous administration of potassium lactate.

Discussion: Clinical studies have shown the crucial roles of IFN-γ for successful cancer immunotherapies involving checkpoint inhibitors and chimeric antigen receptor T cells. The positive implications of this study on the metabolic modulation of IFN-γ activation on heterogeneous tumor cells are discussed.

KEYWORDS

interferon-gamma, nitric oxide, lactate, HIF-1 alpha, tumor

Introduction

IFN-γ is the sole member of type II interferons primarily produced by cells of the immune system, such as T cells and natural killer (NK) cells. IFN-γ is essential in tissue homeostasis, inflammatory responses, and tumor immunosurveillance (1). IFN-γ is involved in progression of several inflammatory diseases. A lack of IFN-γ receptor 1 (IFNGR1) causes severe mycobacterial infections and viral infections caused by herpes virus, respiratory syncytial virus, and parainfluenza virus type 3, with a significant risk of early mortality (2). Immunocompromised children with IFN-γ signaling deficiency are highly susceptible to lethal disseminated bacillus Calmette-Guerin: a condition known as BCGosis and local recurrent nontuberculous mycobacterial infection (3, 4). Other infectious diseases such as leishmaniasis, malaria, influenza, COVID-19, etc., are also alleviated through the IFN-γ-signaling processes (5). However, IFN-γ-hyperactivation negatively impacts several inflammatory and autoimmune diseases: rheumatoid arthritis, multiple sclerosis, Sjogren's syndrome and inflammatory bowel disease (IBD) among others (6–10).

The canonical IFN-γ signaling triggers the JAK-STAT pathway involving JAK2, MEK1/2, Erk1/Erk2, and STAT1α as vital players (11). STAT1α begins transcribing a set of primary response genes, followed by IRF1-mediated secondary response gene expression (12). Several transcription factors from the IFN-γ response, like IRF1 and NF-κB, bind to the *Nos2* promoter and synergistically regulate *Nos2* expression (11, 13). NOS2, an isoform of the NOS enzymes, biosynthesizes Nitric Oxide (NO) from L-arginine and requires several co-factors: reduced nicotinamide-adenine-dinucleotide phosphate (NADPH), flavin adenine dinucleotide (FAD), flavin mononucleotide (FMN), and (6R-)5,6,7,8-tetrahydrobiopterin (BH4) (14). The cellular oxidative state greatly influences the catalytic efficiency of the NOS enzymes. The expression and function of NOS2 biosynthesizing NO is a pivotal marker in IFN-γ signaling in different cell types, including tumors and macrophages (1, 15, 16). NO, a bioactive gaseous molecule with a short half-life, has pleiotropic physiological activities in normal cells and pathophysiological implications in cancer. NO is a component of the IFN-γ signaling response in macrophages and tumors (15–17). IFN-γ signaling induces the transcription of *Nos2* that upregulates the intracellular NOS2 amounts. NOS2 is responsible for the heightened NO production in IFN-γ-activated cancer cells. IFN-γ-modulated genes and responses can be divided into two groups: oxidative and nitrosative stress dependent and oxidative and nitrosative stress independent (15, 16).

The amounts of IFN-γ in the tumor microenvironment, along with the cellular, microenvironmental, and molecular contexts, play major role in the anti-tumor response. Tumors regress under high amounts of IFN-γ through apoptosis and ferroptosis (18) and recombinant IFN-γ therapy against adult T-cell leukemia is approved in Japan (19). Clinical investigations showed that intact IFN-γ signaling is essential for successful immunotherapy against cancer. A genome-wide CRISPR knockout screen in glioblastoma identified that components of the IFN-γ signaling cascade are crucial for the CAR-T cell-mediated killing of tumors (20). Also, clinical responses to immune checkpoint blockade therapy against tumors like melanoma require functional IFN-γ signaling components for tumor regression (21, 22). Therefore, understanding the tumoral response to IFN-γ-signaling is important for understanding host response during cancer immunotherapy.

The progression and functions of IFN-γ signaling are intricately associated with metabolic reprogramming. The production of IFN-γ is tightly regulated by T-cell metabolism, where upregulation of glycolysis favors IFN-γ transcription and translation. GAPDH binds to the 3'-UTR of IFN-γ mRNA to negatively regulate IFN-γ production in naive T-cells (23). IFN-γ production by NK cells upon IL15 activation also depends on elevated glycolysis (24). IFN-γ-mediated classical activation of macrophages toward an inflammatory state requires elevated glycolytic flux and limited reliance on mitochondrial oxidative metabolism (25). IFN-γ-mediated enhanced aerobic glycolysis is essential for clearing Mycobacterial infection in mice (26). These studies led us to investigate the metabolic changes in heterogeneous tumors during IFN-γ activation. Previous studies from our group demonstrated that IFN-γ-activated mouse tumor cells, such as H6 hepatoma and L929 fibrosarcoma, undergo cell cycle arrest and apoptosis (15, 16). In this study, we utilized the *in vitro* model of the IFN-γ-activation of tumor cells to address whether the tumor growth arrest relied on metabolic alterations and dissected the underlying mechanism to identify the key regulatory factors. Finally, we incorporated these key regulatory factors into tumors that do not undergo growth arrest upon IFN-γ-activation. This novel approach led to the growth arrest of the tumors with IFN-γ-activation. It raised the potential of targeting metabolic processes downstream to IFN-γ-activation for an enhanced and effective immunotherapy response against tumors.

Materials and methods

Instruments and reagents

The list of instruments, reagents, their country of origin, and catalogue numbers are listed in Supplementary Table 1.

Cell culture

H6 (hepatoma), Renca (renal adenocarcinoma), RAW 264.7 (monocyte/macrophage), CT26 colon carcinoma, and B16F10 melanoma cell lines were cultured in Dulbecco's modified minimal essential medium (DMEM) containing 10% FBS (27). The media was supplemented with 100 μg/ml penicillin, 250 μg/ml streptomycin, 50 μg/ml gentamycin, 5 μM β-mercaptoethanol and 2 mM glutamine. The cells were maintained at 37°C in a humidified incubator with 5% CO_2 and 95% humidity. H6, Renca,

Abbreviations: DMEM, Dulbecco's modified minimal essential medium, ECAR, extracellular acidification rate, HIF-1α, hypoxia-inducible factor 1α, IFN-γ, interferon-gamma, LNMA, NG-Methyl-L-arginine acetate salt, NO, nitric oxide, NOS, nitric oxide synthase, OCR, oxygen consumption rate.

RAW 264.7 and CT26 cells were procured from Prof. John J. Monaco's laboratory at the University of Cincinnati, Cincinnati, USA and B16F10 was procured from Dr. Sangeeta Bhaskar's laboratory, National Institute of Immunology, New Dehi, India. The detailed features of the cell lines used in this study are tabulated with references in Supplementary Table 2.

Nitrite measurement

NO has a short half-life and reacts with molecular oxygen to form nitrogen dioxide. NO_2 is a reactive molecule that reacts with water to form nitrite and nitrate. The levels of accumulated nitrite were measured to estimate NO production using the Greiss reagent (28). The absorbance was measured at 550 nm using the Tecan microtiter plate reader. The amount of nitrite in the supernatants was calculated from a standard curve of sodium nitrite (1.22 – 625 µM).

Trypan blue dye exclusion assay

The percentage change in cell number was estimated using a Trypan blue dye exclusion assay (16). Cells in the log phase were seeded at an initial density of 10^4 cells per well in a 96-well plate. Post treatment with IFN-γ at indicated time points, cells were harvested using 0.5% Trypsin-EDTA (HiMedia, India) per well. The cells were mixed with an equal volume of 0.4% Trypan blue, and live cells were counted using a hemocytometer.

Seahorse XF analyses

Glycolysis Stress Test and Mitostress test were done to measure the ECAR and OCR from H6 cells. ~$0.8x10^4$ H6 cells were seeded in an 8-well plate in each well, allowed to adhere for 8 h, and treated with IFN-γ for 24 h before being subjected to XF Analyzer (Seahorse Biosciences). The experiments were performed according to the manufacturer's protocol, using the reagents (10 mM D-glucose, 1 mM oligomycin, 50 mM 2-Deoxy D-glucose) for the glycolysis stress test and (1.5 µM oligomycin, 1 µM FCCP, 0.5 µM Rotenone, and Antimycin A) for the mitostress test. The manufacturer supplied the XF media, which was supplemented with 2 mM L-glutamine.

Colorimetric assay for glucose and lactate

Glucose uptake and accumulated lactate were estimated from the cell-free supernatant using a colorimetric glucose estimation kit and lactate assay kit by slightly modifying the manufacturer's protocol to adapt for a microtiter plate reader-based readout. Briefly, for glucose uptake assay, 5 µL of cell-free supernatant, 15 µL of distilled water, and 200 µL of the reaction mix were mixed and incubated for 15 minutes at room temperature. Subsequently, absorbance was measured at 340 nm using a Tecan microtiter plate reader. The cell-free supernatant was diluted in the assay buffer in a 1:1000 dilution for lactate assay. 50 µL of the reaction mixture was added to 50 µL of the diluted supernatant and incubated for 30 minutes at 37°C. The absorbance was recorded at 540 nm at an interval of 10 minutes for lactate assay using a Tecan microtiter plate reader.

RNA isolation and quantitative real-time PCR

RNA isolation from H6 cells was carried out as previously described (15, 27). 3×10^5 of H6 cells were seeded in each well of a 6-well plate. The cells were treated with IFN-γ (10 U/mL) and harvested kinetically. TRI reagent was used to prepare the cell lysates and, subsequently, phenol-chloroform extraction of RNA was performed. Total RNA (1-3 µg) was reverse transcribed to cDNA using a first-strand cDNA synthesis kit and qRT-PCR was performed as mentioned previously (27). The primer sequences are listed in Supplementary Table 3.

Flow cytometry (2-NBDG, ROS, TMRE, MHC class 1)

Glucose uptake and mitochondrial membrane potential were studied using 2-NBDG (29) and TMRE (30) dyes. The intracellular ROS estimation and surface staining of MHC class 1 were performed (16). H6 cells were cultured in 6-well plates at a density of 3×10^5 cells per well and treated with IFN-γ. Cells were incubated with 100 µM 2-NBDG dye in PBS at 37°C water bath for 30 mins in the dark to estimate glucose uptake. Cells were incubated with 150 nM TMRE dye in serum-free DMEM in the dark at room temperature for 10 mins to assess mitochondrial membrane potential. The cells were incubated with 10 µM DCFDA dye at 37°C water bath for 30 mins in the dark to estimate intracellular ROS. Cell pellets were resuspended in 200 µL of PBS in all the cases. MHC class 1 staining was performed by incubating the cells in the blocking buffer {5% FBS and 0.1% (w/v) sodium azide in PBS} for 30 min. The cells were stained with the PE-conjugated anti-MHC Class 1 antibody at the dilution 1:300 for 30 mins with intermittent tapping. The cells were fixed with 4% paraformaldehyde. Data acquisition was performed in the BD FACSVerse™ flow cytometer and analyzed using BD FlowJo™ (BD Biosciences US).

Western blots

Western blot was performed as described (31). 0.5-0.6 million H6 cells were collected, washed in PBS, and lysed in RIPA lysis buffer containing protease and phosphatase inhibitors. The lysates were centrifuged at 14000g for 30 minutes to remove debris, and the supernatant was collected. Protein concentration was determined using the BCA assay. Next, the proteins were separated by SDS-PAGE using a polyacrylamide gel, followed by electrotransfer onto a

PVDF membrane in a semi-dry transfer apparatus. The membrane was then blocked with a blocking solution (e.g., 5% non-fat skim milk in TBST) for 30 minutes on a rocker to prevent non-specific binding. After blocking, the membrane was incubated overnight with a primary antibody specific to the target protein (1:5,000 dilution for HIF-1α or β-Actin antibody, diluted in blocking buffer) at 4°C. Subsequently, the membrane was washed with TBST for 30 minutes at room temperature to remove the unbound primary antibody and then incubated with the secondary antibody conjugated to HRP (1:10,000 dilution in TBST) for 2 hours at room temperature on a rocker. After three washing rounds, the target protein bands were visualized using a chemiluminescent HRP substrate in chemidoc instrument. The band intensities were quantified using Multigauge V3.0 software, and the results were analyzed to determine protein expression levels.

Statistical analyses

GraphPad Prism software version 8.0.2 was used for generating graphical representations and conducting statistical evaluations. Data are represented as the mean ± standard deviation of the mean (SD). A quantile-quantile (QQ) plot assessed data distribution and skewness. Subsequently, statistical analyses were executed employing ordinary One-way Analysis of Variance (ANOVA) paired with Sidak's multiple comparisons tests and two-way ANOVA coupled with Tukey's multiple comparisons tests. In the context of statistical significance, various symbols were utilized: (ns) denoting non-significant differences and (*), (**), (***), and (****) signifying statistical differences with p-values less than 0.05, 0.01, 0.001, and 0.0001, respectively, among the specified comparisons (27).

Results

IFN-γ activation increases NO and glycolysis-mediated extracellular acidification with growth reduction in H6 cells

Previous research from our group demonstrated that H6 cells undergo cell cycle arrest and apoptosis upon activation by IFN-γ, which is dependent on intracellular NO and ROS (15, 16). In this study, we attempted to test whether the cytostatic fate of tumors upon IFN-γ-activation is associated with metabolic reprogramming. The cellular respiratory and metabolic alterations often lead to the release of gaseous byproducts and metabolites that can influence the extracellular pH (32, 33). Initially, we used the H6 cells as a model to study IFN-γ activation (15, 16) and examined the pH of the cell culture medium. The cell culture medium contains phenol red as a pH indicator. After 24 hours of IFN-γ-activation, the cell-free supernatant of H6 cells was visibly more orange compared to the untreated control (Figure S1B). The phenomenon did not cause any noticeable cytomorphological change in the H6 cells (Figure S1A). The pH measurement revealed that the mean pH of cell-free supernatant from IFN-γ-treatment was 6.64 ± 0.03, less than the untreated control, which was 6.84 ± 0.02 (Figure S1C). The pH scale is logarithmic, meaning that a change of 0.2 corresponds to a twofold increase in acidity, which may be physiologically significant.

One possibility was that the increased cell growth may enhance extracellular acidification upon IFN-γ-activation. The nitrite and lactate production significantly increased post-24 hours of IFN-γ-activation. However, the total cell number reduction was not significant due to variations in data points despite an overall trend (Figure S1D). Therefore, the data was expressed as the percent cell number change and the statistically significant cell number reduction was obtained after 24 hours of activation (15, 16). The *in vitro* acidification of IFN-γ-activated H6 cells was also accompanied by a kinetic increase in nitrite production. The nitrite amounts were normalized to the percent cell number values for a fair analysis. The level of nitrite significantly increased after 12 and 24 hours of IFN-γ-activation (Figure 1A).

It was important to address the source of extracellular acidification during IFN-γ-activation of H6 cells. We used multiple approaches to address this aspect: the TMRE-based flow cytometric assessment tested mitochondrial membrane potential and the seahorse mitostress test assessed mitochondrial oxygen consumption rate (OCR). IFN-γ-activation of H6 cells significantly reduced mitochondrial membrane potential and OCR. The reduced OCR in IFN-γ-activated H6 cells was significantly less responsive to pharmacological inhibitors of mitochondrial function, i.e., oligomycin, FCCP, rotenone, and antimycin (Figure 1B). Therefore, these assessments indicated that the compromised mitochondrial function might not increase CO_2 release upon IFN-γ-activation.

We further tested whether the glycolytic mean of metabolic acidosis contributes to the IFN-γ-induced enhanced extracellular acidification. The glycolysis stress test revealed that glucose-starved IFN-γ-activated H6 cells display a significantly heightened extracellular acidification rate (ECAR) upon glucose injection. The ECAR enhancement did not alter upon F_o-F_1 inhibition by oligomycin, proving no involvement of mitochondrial ATP production. The inhibition of hexokinase dampened ECAR, ultimately leveling the untreated H6 cells (Figure 1C). In conclusion, the IFN-γ-mediated heightening of ECAR remarkably depended on glycolysis. The H6 cells consumed glucose and produced lactate in significantly higher amounts after 24 hours of IFN-γ-activation (Figure 1A). Therefore, IFN-γ-activation rewired the cellular metabolism to augment the glycolytic production of lactate and skewed mitochondrial functions.

IFN-γ activation boosts NO and ROS formation, enhancing glycolytic flux and upregulating lactate production from H6 cells

Next, we asked whether NOS2-induced NO plays any regulatory role in enhancing the IFN-γ-mediated glycolytic flux (15). The pharmacological inhibitors of NOS function, i.e., N^{ω}-

10.3389/fimmu.2023.1282653

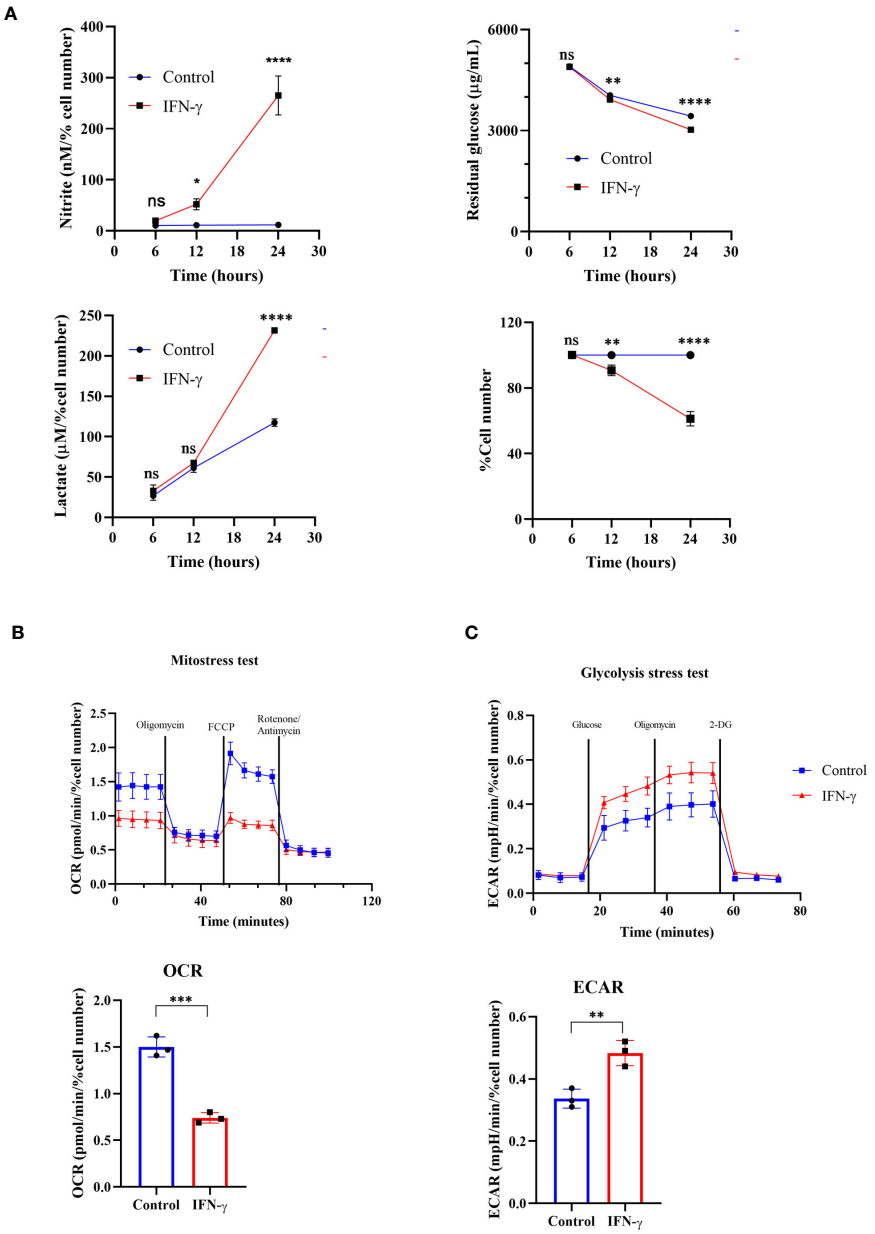

FIGURE 1
IFN-γ-activation of H6 cells increases glycolytic flux and compromises mitochondrial function. H6 hepatoma cells were seeded in a 6-well plate and treated with 10 U/mL IFN-γ for the indicated time points. The cell numbers were counted, and the cell-free supernatant was collected and assayed for nitrite, residual glucose, and lactate. The nitrite and lactate levels were normalized to the percent cell number **(A)**. The Seahorse XF analysis of the H6 cells was performed post-IFN-γ-activation for 24 hours. The pharmacological modulators were sequentially injected as indicated. The mitostress test with the OCR from the 4th measurement **(B)** and the glycolysis stress test with the ECAR from the 3rd measurement **(C)** are shown. Statistical analyses in this study were conducted utilizing two-way ANOVA in conjunction with Tukey's multiple comparisons tests **(A)** and unpaired t-tests **(A–C)**. The notation "ns" indicates non-significant differences, while (*), (**), (***), and (****) denote statistical significance levels of $p < 0.05$, $p < 0.01$, $p < 0.001$, and $p < 0.0001$, respectively, for comparisons between the groups specified. Each data point is a representative observation derived from an independent experiment. The data are expressed as the mean ± standard deviation based on 3 to 5 independent experiments.

Methyl-L-arginine (LNMA; inhibits all NOS isoforms) or 1400W (specifically inhibits NOS2), were added in the presence of IFN-γ (15, 16, 34). Both the NOS inhibitors significantly reduced the IFN-γ-induced NO and ROS production and rescued cell growth reduction (Figures 2A, D, S2A). The efficiency of glucose uptake was tested using 2-NBDG-based flow cytometry and measuring the residual glucose amounts in the cell-free supernatant. NOS inhibition significantly reduced the glucose uptake and lactate production of IFN-γ-activated H6 cells (Figures 2B, C, S2B). Therefore, IFN-γ-induced NO production dominantly increases the glycolytic flux in H6 cells.

Subsequently, we asked whether lactate production can be enhanced by further elevation of intracellular NO. SNAP, a NO-donor compound, was added to the H6 cells in the presence of IFN-γ. The exogenous NO-donation approach did not elevate the IFN-γ-induced production of nitrite. The level of lactate and percent cell

10.3389/fimmu.2023.1282653

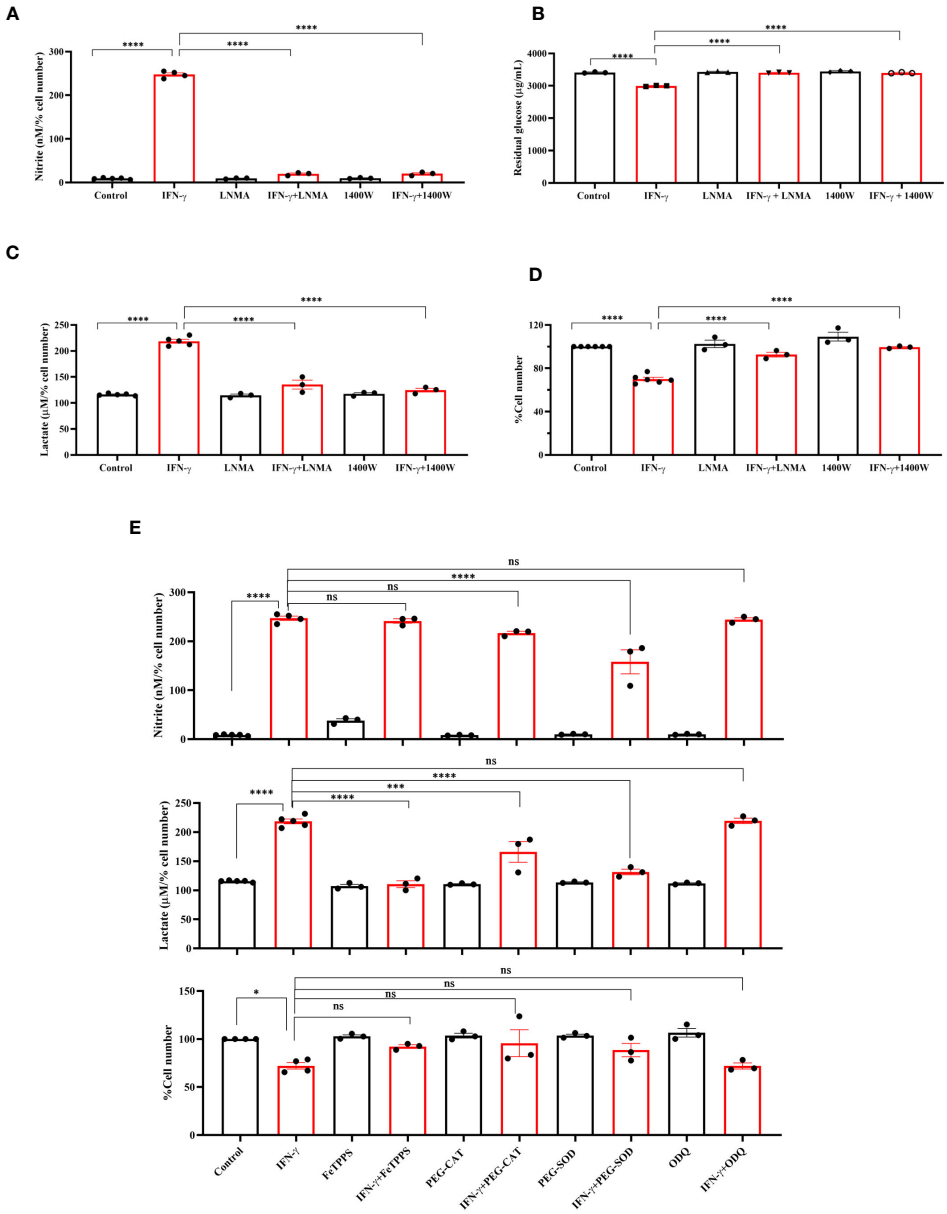

FIGURE 2
IFN-γ-activated augmentation of glycolytic flux is NO and ROS-dependent in H6 cells. H6 cells were treated with 10 U/ml IFN-γ and incubated alone or with pharmacological inhibitors of NOS enzymes (LNMA at 200 uM and 1400W at 6 uM) for 24 hours to inhibit NO biosynthesis. The nitrite levels were measured from the cell-free supernatants and normalized to the percent cell number **(A)**. The residual glucose concentrations in the cell-free supernatant were measured after 24 hours of IFN-γ-activation of the H6 cells **(B)**. The lactate concentrations were measured in the same cell-free supernatant and normalized to percent cell number **(C)**. The cell numbers were counted and represented as the percent cell number **(D)**. The H6 cells were treated with 10 U/ml IFN-γ and incubated alone or with the peroxynitrite quencher (FeTPPS at 50 uM), inhibitors of ROS production (PEG–CAT at 100 U/ml and PEG–SOD at 50 U/ml) and soluble guanylate cyclase inhibitor ODQ at 20 uM for 24 hours. The cell numbers were counted and represented as the percent cell number. The nitrite and lactate concentrations were measured in the cell-free supernatant and normalized to percent cell number. **(E)**. Statistical analyses in this study were conducted utilizing ordinary one-way ANOVA in conjunction with Sidak's multiple comparisons tests. The notation "ns" indicates non-significant differences, while (*), (***), and (****) denote statistical significance levels of $p < 0.05$, $p < 0.001$, and $p < 0.0001$, respectively, for comparisons between the groups specified. Each data point is a representative observation derived from an independent experiment. The data are expressed as the mean ± standard deviation based on 3 to 5 independent experiments.

number remained unaffected (Figure S3A). Therefore, we opted for an alternative strategy involving the concept of 'arginine paradox'. In this phenomenon, increased arginine availability leads to increased NO production despite a theoritical intracellular saturation of L-arginine for the NOS enzyme activity (35). H6 cells were treated with L-arginine in varying concentrations in the presence of IFN-γ for 24 hours. This approach successfully elevated IFN-γ-induced NO production in a concentration-dependent manner. However, the IFN-γ-induced increased lactate production and reduced cell growth remained unaffected despite the significant increase in NO production (Figures S3B, C). These results suggest that the NO-mediated elevation of lactate

production occurs at maximum saturation upon the IFN-γ-activation of H6 cells.

One of the mechanisms of the effects of NO is exerted by activating intracellular soluble guanylate cyclase (sGC) and subsequent upregulation of cyclic GMP (cGMP) (36). We asked whether the cGMP upregulation is responsible for enhancing lactate release. ODQ, a pharmacological inhibitor of sGC, did not affect the IFN-γ-induced nitrite and lactate production and reduction in percent cell number (Figure 2E). Therefore, cGMP-activation was not involved in the IFN-γ-mediated enhancement of lactate production. Next, we asked whether NO-induced ROS levels affect the lactate release in the IFN-γ-activated H6 cells (16). Peroxynitrite, hydrogen peroxide, and superoxide radical levels were quenched using FeTPPS, pegylated catalase (PEG-CAT), and pegylated superoxide dismutase (PEG-SOD), respectively. PEG-SOD partially but significantly reduced NO production, indicating that the oxidative environment created by superoxide radicals promoted NO biosynthesis. The IFN-γ-mediated cell growth reduction was partially but non-significantly rescued in the presence of all three RNS and ROS quenchers. All three RNS and ROS quenchers significantly reduced the IFN-γ-mediated lactate production (Figure 2E). In conclusion, IFN-γ-mediated NO and subsequent ROS production are responsible for IFN-γ-mediated increased lactate production in H6 cells.

IFN-γ-activated glycolytic flux augmentation promotes NO formation and reduces cellular growth of H6 cells

The IFN-γ-mediated enhancement of lactate release raised the question of why the cells undergo metabolic reprogramming toward the induction of glycolysis and what the cells gain from the glycolytic dependency. The question was addressed using pharmacological inhibition of several nodes of the glycolytic pathway: 2-deoxyglucose (2-DG, an inhibitor of hexokinase), GSK2837808A (an inhibitor of lactate dehydrogenase A or LDHA), and AR-C155858 (an inhibitor of monocarboxylate transporter 1-4 or MCT1-4). 2-DG, GSK2837808A, and AR-C155858 block the first step of glycolysis, lactate production, and lactate shuttling in and out of the cells, respectively. All the inhibitors significantly reduced glucose uptake and lactate production and release by the IFN-γ-activated H6 cells (Figures 3C, E, S4B). However, none of the inhibitors affected the IFN-γ-mediated induction of MHC class 1 surface expression and reduction in mitochondrial membrane potential (Figures 3D, S4A, C). All the inhibitors partially but significantly reduced the IFN-γ-induced NO production (Figure 3A) and 2-DG significantly reduced the IFN-γ-induced ROS production (Figure 3B). Importantly, all the inhibitors partially but significantly rescued the IFN-γ-mediated percent cell number reduction (Figure 3F). In conclusion, the IFN-γ-activated H6 cells produce NO and ROS to enhance glycolysis. Most likely, the cells harness the utilities of IFN-γ-induced glycolytic flux augmentation to promote NO production further and reduce cellular growth.

To address the role of lactate in the IFN-γ signaling responses, potassium lactate was added along with IFN-γ to the H6 cells. Potassium lactate did not reduce the pH of the cell culture medium and was preferred over lactic acid to avoid the effects of pH reduction (37). Potassium lactate, upon IFN-γ-activation, completely rescued the extracellular acidification and pH reduction, from 6.65 ± 0.04 in IFN-γ to 6.97 ± 0.05 in the combination of IFN-γ and potassium lactate. Potassium lactate significantly reduced the IFN-γ-mediated enhancement of intracellular ROS and glucose uptake (Figures 3B, C, S4B). These indicate that potassium lactate reduced the glucose dependency of the IFN-γ-activated cells and most likely, served as an alternative carbon source to rewire the metabolism. Notably, the rewired metabolism significantly augmented the IFN-γ-induced NO production and cell growth reduction (Figures 3A, F). These observations indicate that the IFN-γ-activated H6 cells may utilize the heightened production of lactate to promote IFN-γ signaling in an autocrine manner.

IFN-γ promotes HIF-1α stabilization and transcriptional upregulation of HIF-1α target glycolytic genes in H6 cells

Previous reports suggested that pharmacological donation of NO and elevation of intracellular ROS can activate the hypoxia signaling process by inhibiting the prolyl hydroxylase (PHD) enzyme. Also, HIF-1α is a well-known regulator of glycolytic flux in tumor cells (38). Therefore, we tested whether the IFN-γ-activation of H6 cells stabilizes HIF-1α and upregulates glycolytic gene expression. RT-qPCR-based gene expression analysis revealed that IFN-γ-activation significantly upregulated several well-known members of IFN-γ-activated gene expression. The transcription of *Irf1* and *Nos2* was significantly upregulated after 6 and 12 hours of activation. *Cd274* was significantly upregulated after 6 hours of IFN-γ-activation. Along with the well-known gene expression profile, IFN-γ-activation also significantly upregulated *Hif1a* transcription after 6 and 12 hours (Figure 4A). Immunoblot analysis of HIF-1α revealed that the HIF-1α levels were significantly increased after 12 hours of IFN-γ-activation in H6 cells (Figure 4B), indicating that the upregulation of intracellular HIF-1α is regulated at both mRNA and protein levels.

A list of HIF-1α-induced differentially upregulated genes ($\log_2$ fold change ≥ 1.5) was obtained from the NCBI GEO dataset (GSE98060) (39), analysed with GEO2R, and imported into the String tool of EMBL-EBI. A protein-protein interaction (PPI) network was constructed using the String tool to identify the functional enrichment of the topmost interconnected cluster and Cytoscape software analyzed the network. The network had 354 nodes, 48 edges, an average node degree of 0.271, with an average local clustering coefficient of 0.0998. KEGG pathway analysis showed that the glycolysis pathway is the second most enriched pathway after the HIF-1α signaling pathway (Supplementary Table 4). The K-means method and MCODE-based computation of network clustering identified that the topmost interconnected

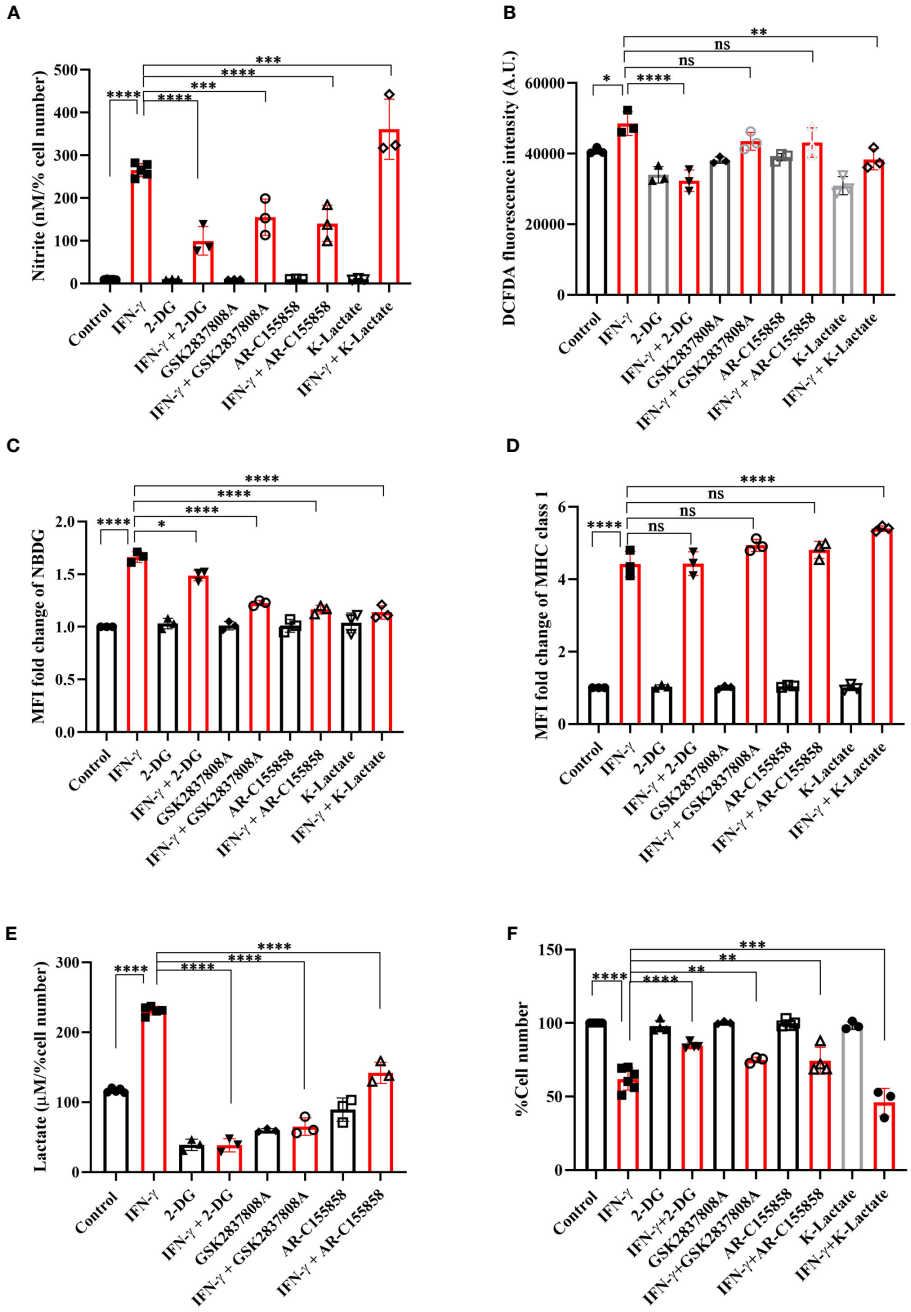

FIGURE 3
IFN-γ-mediated enhanced glycolysis fuels IFN-γ signaling responses by increasing NO and decreasing cell number. H6 cells were treated with 10 U/ml IFN-γ and incubated alone or with pharmacological modulators of glycolysis (2-DG, a hexokinase inhibitor at 2.5 mM; GSK2837808A, a lactate dehydrogenase inhibitor at 125 nM; AR-C155858, a monocarboxylate transporter inhibitor at 6 nM and K-lactate as a metabolic reprogramming agent at 10 mM). The cell-free supernatants were collected after 24 hours, and the level of nitrite and lactate were estimated **(A, E)**. The cell numbers were counted to derive the percent cell number **(F)**. The levels of nitrite and lactate were normalized to the percent cell number. The intracellular ROS was measured using a Tecan microplate reader from 0.1 million cells/well upon DCFDA staining for 30 minutes **(B)**. The IFN-γ-activated H6 cells were assayed for glucose uptake and surface expression of MHC class 1 using flow cytometry in the presence of the glycolysis modulators. The cells were incubated with 100 µM 2-NBDG for 30 minutes, and flow cytometric analysis of glucose uptake was performed **(C)**. The cells were stained with an antibody to MHC class 1, and flow cytometric analysis of the surface expression of MHC Class 1 was performed **(D)**. Statistical analyses in this study were conducted utilizing ordinary one-way ANOVA in conjunction with Sidak's multiple comparisons tests. The notation "ns" indicates non-significant differences, while (*), (**), (***), and (****) denote statistical significance levels of $p < 0.05$, $p < 0.01$, $p < 0.001$, and $p < 0.0001$, respectively, for comparisons between the groups specified. Each data point is a representative observation derived from an independent experiment. The data are expressed as the mean ± standard deviation based on 3 independent experiments.

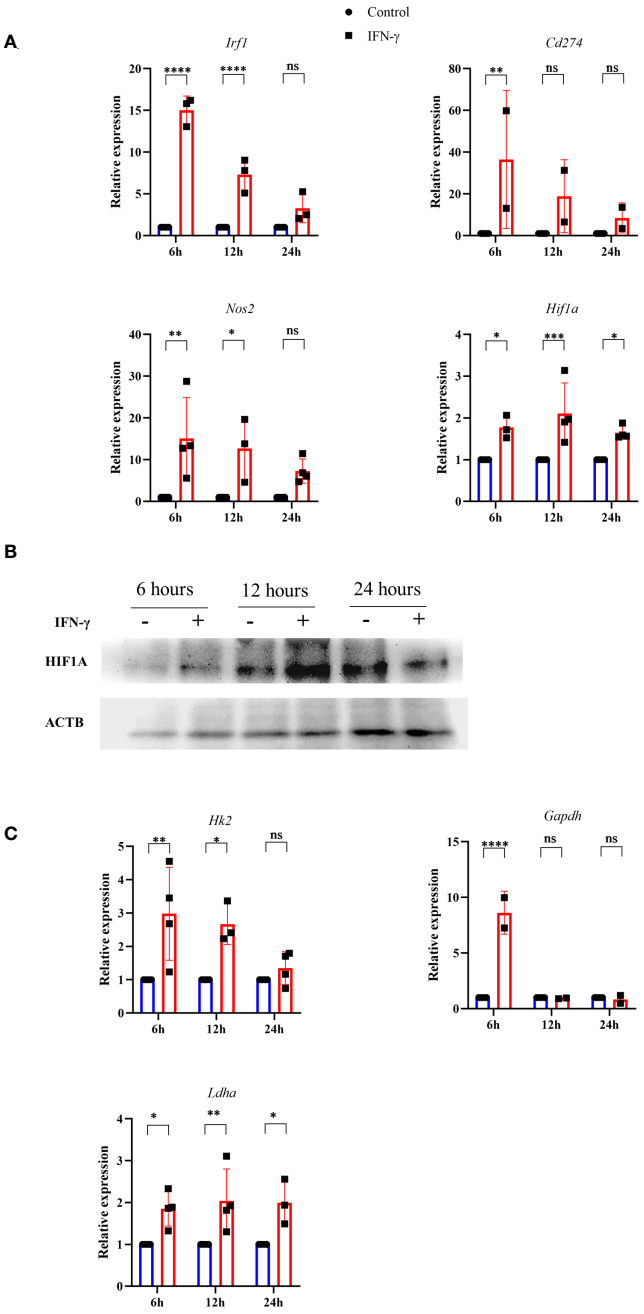

FIGURE 4
IFN-γ-activation stabilizes HIF-1α and induces several HIF-1α-responsive glycolytic genes. H6 cells were treated with 10 U/ml IFN-γ in a 6-well plate for the indicated time points, and total RNA was extracted. RT-qPCR was performed to quantify the relative expression of *Irf1*, *Nos2*, *Cd274*, and *Hif1a* **(A)**. The cells were lysed at the indicated time, and immunoblot was performed to quantify the HIF-1α intracellular protein amounts. β-Actin was used as the loading control **(B)**. The relative mRNA expression of several HIF-1α target genes, such as *Hk2*, *Gapdh*, and *Ldha*, was also quantified using RT-qPCR **(C)**. Statistical analyses in this study were conducted utilizing two-way ANOVA in conjunction with Tukey's multiple comparisons tests. The notation "ns" indicates non-significant differences, while (*), (**), (***), and (****) denote statistical significance levels of $p < 0.05$, $p < 0.01$, $p < 0.001$, and $p < 0.0001$, respectively, for comparisons between the groups specified. Each data point is a representative observation derived from an independent experiment. The data are expressed as the mean ± standard deviation based on 3 to 4 independent experiments.

regulatory network of HIF-1α majorly consists of several glycolytic genes (Figures S5A, B). Based on these data, we asked whether the IFN-γ-induced glycolytic flux enhancement is associated with the transcriptional upregulation of HIF-1α-target glycolytic genes: *Hk2*, *Gapdh*, and *Ldha*. *Hk2*, *Gapdh*, and *Ldha* encode hexokinase 2, glyceraldehyde-3-phosphate dehydrogenase, and lactate dehydrogenase a, respectively. All three glycolytic genes were significantly upregulated after 6 hours of IFN-γ-activation. *Hk2* and *Ldha* were significantly upregulated after 12 hours of IFN-γ-activation (Figure 4C). HIF-1α is known to upregulate *Vegfa* to promote tumor angiogenesis. However, the RT-qPCR-based analysis revealed that *Vegfa* was not differentially regulated in

IFN-γ-activated H6 cells (Figure S6C). These indicate that the IFN-γ-induced HIF-1α-mediated gene expression does not mimic the canonical hypoxia-induced HIF-1α gene expression signature but involves specific ones, especially glycolytic genes. Lactate dehydrogenase a (LDHA) and Lactate dehydrogenase b (LDHB) perform opposite functions. LDHA promotes pyruvate oxidation to lactate, whereas LDHB promotes lactate reduction to pyruvate (40). *Ldhb* was also not differentially regulated upon IFN-γ-activation, whereas *Ldha* was significantly upregulated 24 hours post-activation by IFN-γ (Figures 4C, S6C). These observations indicate that the glycolytic flux upregulation is accompanied by *Hif1a* expression, HIF-1α stabilization, and HIF-1α-targeted glycolytic gene expression.

The IFN-γ-induced function of HIF-1α promotes NO and ROS production, enhances glycolytic flux, and lowers cellular growth

The functional roles of HIF-1α in the IFN-γ-induced glycolytic flux was addressed using pharmacological approaches: chetomin (an inhibitor of HIF-1α) and DMOG (a pharmacological HIF-1α stabilizer) were used in IFN-γ signaling. The HIF-1α stabilizer DMOG did not affect the IFN-γ-induced NO and ROS production, mitochondrial membrane potential, MHC class 1 surface expression, glucose uptake, and cell growth reduction (Figures 5A–D, F, S7). However, DMOG significantly increased IFN-γ-induced lactate release, indicating that the IFN-γ-activated H6 cells contain more room for glycolytic flux enhancement (Figure 5E). The HIF-1α inhibitor chetomin reduced IFN-γ-induced NO and ROS production and glycolytic flux and rescued cell growth reduction significantly (Figures 5A–E, S7C, D). Hence, these observations demonstrate that HIF-1α partially regulates NO and ROS production, whereas it strongly regulates the IFN-γ-induced glycolytic flux enhancement. More importantly, HIF-1α significantly rescued IFN-γ-induced cell growth reduction (Figure 5F). Therefore, HIF-1α stabilization substantially enhances glycolytic flux downstream of NO, thereby reducing cell growth.

The addition of exogenous potassium lactate in the presence of IFN-γ decreases cellular growth in non-NO-producing cells

The NO-dependent regulation of glycolytic flux enhancement upon IFN-γ-activation of H6 cells led us to ask whether the process is also observed in other tumor cell lines. Raw 264.7 (monocyte/macrophage) and Renca (renal adenocarcinoma) tumor cell lines produced NO and reduced cell number post IFN-γ activation, phenocopying the response of the H6 cell line. IFN-γ-induced Raw 264.7 and Renca cells also produced heightened amounts of lactate (Figures 6A, B).

Two non-NO-producing cell lines CT26 (colon carcinoma) and B16F10 (melanoma) did not increase NO and reduce cell growth upon IFN-γ-activation. None of the non-NO-producing cell lines increased lactate; however, B16F10 showed slight but significant reduction in lactate production (Figures 6C, D). Therefore, we asked whether the reconstitution of the IFN-γ-inducible missing components, such as NO, HIF-1α, and lactate, can sensitize the resistant non-NO-producing cell lines into phenocopying the NO-producing ones by reducing cell growth. The differences between CT26 and B16F10 at the basal level and IFN-γ-activation were initially investigated. At basal growth conditions, the B16F10 cells exhibited significantly lesser MHC class 1 surface expression and cell growth but higher lactate production than the CT26 cells (Figure S8). Notably, IFN-γ-activated B16F10 cells exhibited much higher MHC class 1 induction regarding fold change (~20-55-fold increase) than CT26 cells (~2-5-fold increase). This observation indicated that the strength of response to IFN-γ in B16F10 cells is remarkably greater compared to CT26 cells (Figure S9A).

NO, HIF-1α, and lactate were incorporated in CT26 and B16F10 cells using SNAP, DMOG, and potassium lactate. None of these pharmacological modulators affected IFN-γ-induced MHC class 1 surface expression in both CT26 and B16F10 cell lines (Figure S9A). Apart from SNAP, none of the pharmacological modulators affected the NO amounts (Figure S9B). Lactate levels and percent cell number remained unaffected upon adding SNAP in the presence of IFN-γ in B16F10 cells. DMOG did not affect the lactate levels and cell growth in CT26 cells upon IFN-γ-activation; however, it significantly increased lactate and reduced cell growth in B16F10 cells (Figures 7A, B). Most importantly, the exogenous addition of lactate into IFN-γ-activated CT26 and B16F10 cells significantly decreased the percent cell number, reducing cell growth (Figure 7B).

Discussion

An optimal IFN-γ-activation is well-known to trigger anti-tumor responses in cancer cells by inhibiting angiogenesis, increasing Treg fragility, inducing tumor senescence, and triggering apoptosis and ferroptosis (18). In this study, we demonstrated that IFN-γ-activated H6 cells underwent impairments in mitochondrial functions, glycolytic flux elevation, and extracellular acidification (Figures 1, S1). The primary modes of extracellular acidification are respiratory or metabolic. Enhancing mitochondrial function can release high levels of CO_2 and contribute to respiratory acidification. However, efficient utilization of O_2 under optimal mitochondrial membrane potential is necessary for CO_2 release. Therefore, the reduced OCR upon IFN-γ-activation of H6 cells indicated that the IFN-γ-induced augmented glycolysis in H6 cells contributed to the extracellular acidification. The mitochondria of IFN-γ-activated H6 cells exhibited less mitochondrial membrane potential and oxygen consumption, indicating reduced dependency on mitochondrial oxidative phosphorylation for ATP production. The increased acidity can hamper enzyme functions and biochemical reactions. It is well-known that reducing the normal physiological pH by 0.1-0.2 in the human body leads to severe

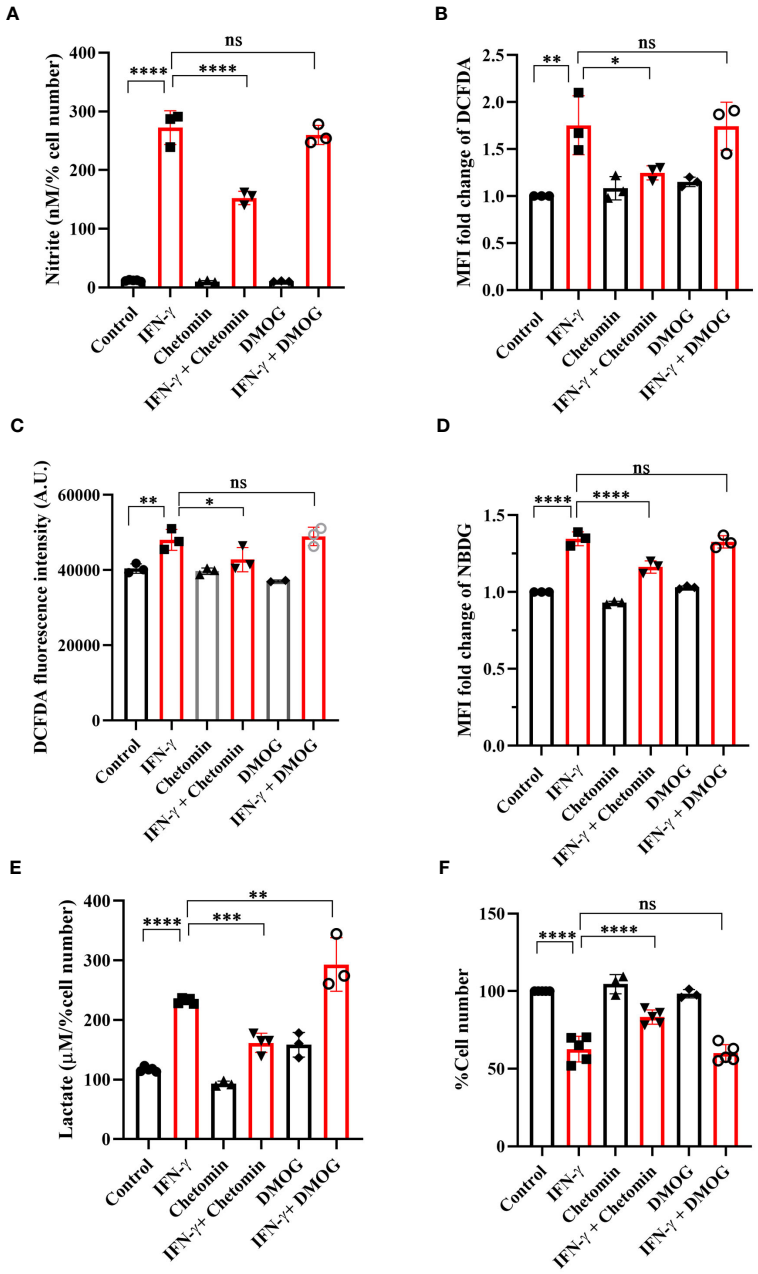

FIGURE 5
IFN-γ-activated augmentation of glycolytic flux is dependent on HIF-1α in H6 cells. H6 cells were treated with 10 U/ml IFN-γ for 24 hours. The IFN-γ-activated cells were incubated alone or with pharmacological modulators of HIF-1α function (Chetomin, an inhibitor of HIF-1α at 12.5 nM, and DMOG, a stabilizer of HIF-1α at 0.5 uM). The cell-free supernatant was collected and the levels of nitrite and lactate were estimated in the cell-free supernatant. The nitrite and lactate levels are normalized to percent cell number **(A, E)**. The IFN-γ-activated H6 cells were assayed for intracellular ROS by incubating the cells with 10 μM DCFDA for 30 minutes. The analyses of intracellular ROS were performed using flow cytometry **(B)** and Tecan microplate reader-based estimation **(C)**. The cells were incubated with 100 μM 2-NBDG for 30 minutes, and flow cytometric analysis of glucose uptake was performed **(D)**. The cell number was counted to derive the percent cell number **(F)**. Statistical analyses in this study were conducted utilizing ordinary one-way ANOVA in conjunction with Sidak's multiple comparisons tests. The notation "ns" indicates non-significant differences, while (*), (**), (***), and (****) denote statistical significance levels of $p < 0.05$, $p < 0.01$, $p < 0.001$, and $p < 0.0001$, respectively, for comparisons between the groups specified. Each data point is a representative observation derived from an independent experiment. The data are expressed as the mean ± standard deviation based on 3 to 5 independent experiments.

acidosis and can be fatal (41). These observations indicated that IFN-γ-activated H6 cells phenocopy a similar metabolic rewiring, observed in activated macrophages to meet the cytostatic fate. The reduced tumor growth is less likely due to reduced pH because adding potassium lactate upon IFN-γ-activation of H6 cells reduced tumor growth without reducing pH (Figure 3F). These led us to investigate the detailed mechanism behind IFN-γ-induced glycolytic flux elevation.

NO derived from the non-malignant stromal components of tumors or NO-donor pharmacological agents often promotes

10.3389/fimmu.2023.1282653

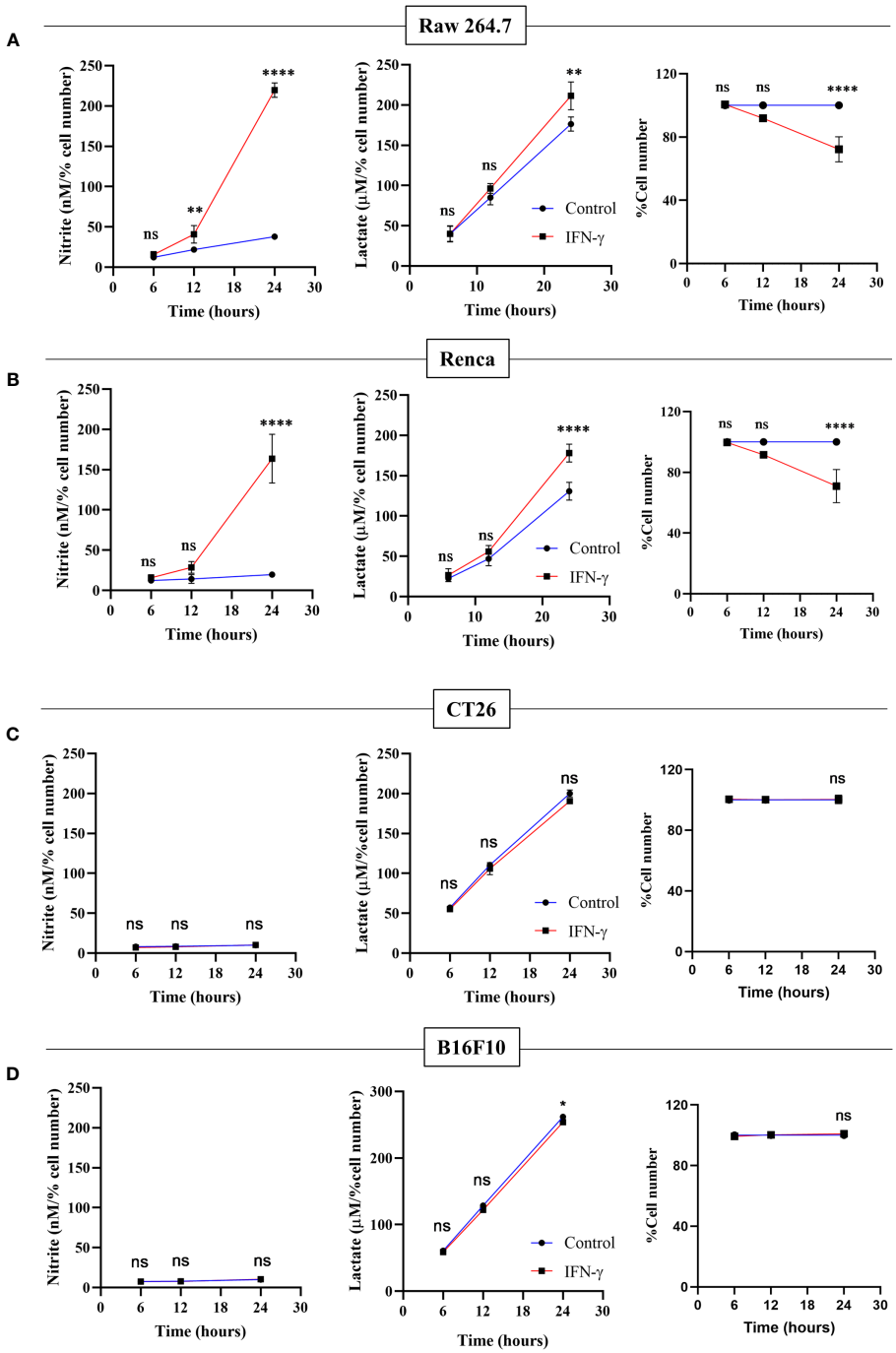

FIGURE 6
Only IFN-γ-activated NO-producing tumor cells increase lactate production and reduce cell number. Raw 264.7 **(A)**, Renca **(B)**, CT26 **(C)**, and B16F10 **(D)** cell lines were treated with 10 U/mL IFN-γ in a 24-well plate. The cell culture medium was collected kinetically. The levels of nitrite and lactate were measured from the cell-free supernatant. The cell number was counted to derive the percent cell number. The statistical analyses were performed using two-way ANOVA with Tukey's multiple comparisons tests for comparing nitrite and lactate levels and unpaired t-test for comparing the percent cell number. The notation "ns" indicates non-significant differences, while (*), (**), and (****) denote statistical significance levels of $p < 0.05$, $p < 0.01$, and $p < 0.0001$, respectively, for comparisons between the groups specified. Each data point is a representative observation derived from an independent experiment. The data are expressed as the mean ± standard deviation based on 3 to 5 independent experiments.

tumor progression by angiogenesis, defective P53 functions, histone methylation, and metastasis (42). However, intratumoral NO synthesis by NOS2 and peroxynitrite, a primary byproduct of excessive intracellular NO production, inhibits the mitochondrial Electron Transport System (ETS) complexes, derails the efficient electron transfer process to molecular oxygen, and produces mitochondrial superoxide radicals (43). Superoxide radicals react with water molecules to produce hydrogen peroxide. Therefore,

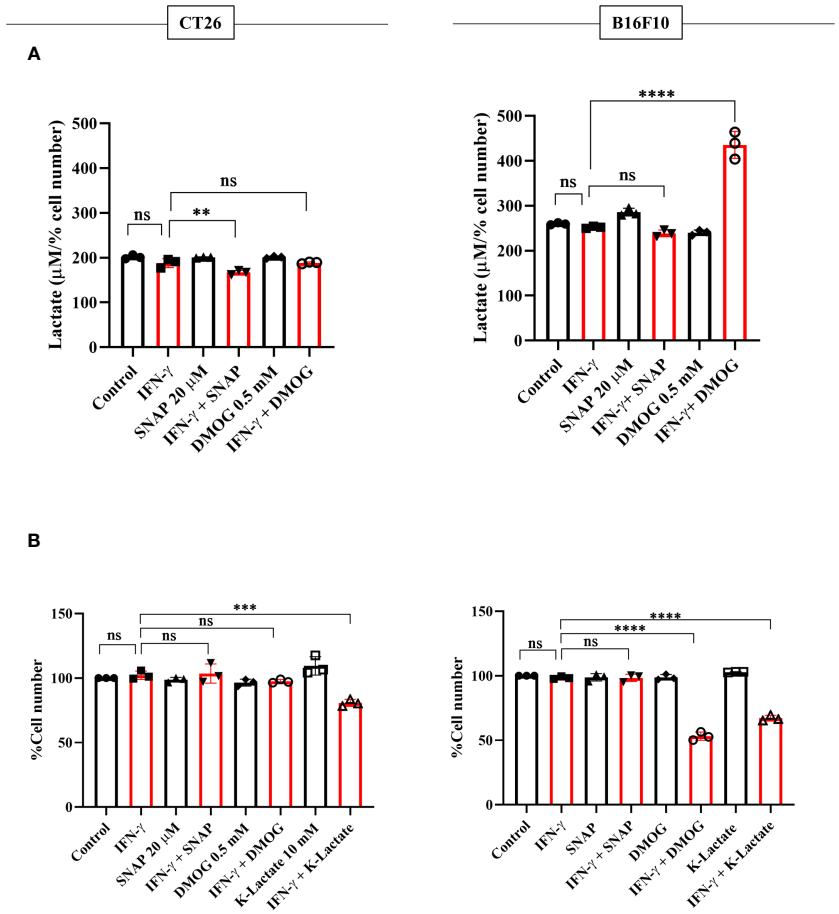

FIGURE 7
K-lactate in the presence of IFN-γ lowers the growth of non-NO-producing cell lines, CT26 and B16F10 cells. CT26 and B16F10 cells were treated with 10 U/ml IFN-γ and incubated alone or with pharmacological modulators (SNAP, an NO donor at 25 µM; DMOG, a stabilizer of HIF-1α at 0.5 µM and K-lactate as a metabolic reprogramming agent at 10 mM) for 24 hours. The level of lactate was measured from the cell-free supernatant. The lactate level was normalized to the percent cell number **(A)**. The cell number was counted to derive the percent cell number **(B)**. Statistical analyses in this study were conducted utilizing ordinary one-way ANOVA in conjunction with Sidak's multiple comparisons tests. The notation "ns" indicates non-significant differences, while (**), (***), and (****) denote statistical significance levels of $p < 0.01$, $p < 0.001$, and $p < 0.0001$, respectively, for comparisons between the groups specified. Each data point is a representative observation derived from an independent experiment. The data are expressed as the mean ± standard deviation based on 3 independent experiments.

excessive NO production increases intracellular peroxynitrite and ROS levels. The elevated NO-induced nitrosative and oxidative damage triggers the caspase activation and apoptosis in NO-producing tumor cells (16). This study led us to evaluate the IFN-γ response in tumor cells and categorize NO-producing tumor cells: H6, Raw264.7, and Renca, and non-NO-producing tumor cells: CT26 and B16F10. All IFN-γ-induced NO-producing cells produced heightened lactate amounts, accompanied with lowered cell growth, whereas non-NO-producing cells did not (Figures 1, 6). The IFN-γ-induced glycolytic flux enhancement in H6 cells depended on the inducible NO production (Figures 2B, C). Elevated ROS also contributed to heightened lactate production in these cells (Figure 2E). Furthermore, the increased glycolysis also promoted NO and ROS production in H6 cells, indicating the presence of reciprocal regulation between these processes (Figures 3A, B). Reciprocal regulation might strengthen the IFN-γ-signaling, culminating in apoptosis and cellular growth reduction.

Cellular oxygen sensing is tightly regulated to promptly adapt to hypoxic conditions by inducing glycolytic processes and meeting bioenergetic demands. Intracellular HIF-1α is hydroxylated by the Prolyl hydroxylases (PHDs) and degraded under normoxic conditions. On the other hand, low oxygen amounts in hypoxia limit oxygen availability for the PHD enzyme, leading to reduced hydroxylation of HIF-1α and its intracellular stabilization. HIF-1α is paramount in inducing glycolytic gene transcription and boosting glycolysis to produce ATP under hypoxia (44). However, HIF-1α can also be stabilized under immune non-hypoxic conditions by the influence of high amounts of NO and ROS (45). IFN-γ-mediated inflammatory processes stabilize HIF-1α in a non-hypoxic manner. The IFN-γ-mediated HIF-1α stabilization is beneficial during Mycobacterial infections by inducing metabolic reprogramming toward glycolysis and bacterial clearance (26). However, this regulation can be harmful during other conditions, such as the inflammation of the aortic valve (46). Our study showed that IFN-γ-

activated H6 cells transcriptionally upregulated *Hif1a* transcription and increased intracellular HIF-1α levels kinetically (Figure 4). The HIF-1α stabilization in H6 cells may have happened due to NO and ROS induction by IFN-γ. The HIF-1α might self-regulate its transcription to strengthen its actions. Alternatively, IFN-γ may induce the *Hif1a* transcription to increase intracellular HIF-1α levels and enhance glycolytic flux. IFN-γ reduced tumor growth by increasing NO and stabilizing HIF-1α to enhance glycolytic flux in H6 cells. The HIF-1α-induced glycolytic flux enhancement contributed to NO production, probably by supplying the substrate and various cofactors to NOS2 and contributing to ROS generation (Figure 5). Clinical datasets of inflammatory diseases revealed that the gene expression of HIF-1α and NOS2 are correlated in several diseases, like colon inflammation, Crohn's disease, and mixed osteosarcoma (Figure S5). These observations indicate that IFN-γ-induced *Nos2* and *Hif1a* transcription were correlated and may be functional in tissue inflammatory diseases.

In mammalian cells, lactate production increases during intense exercise and ischemia when the demand for ATP and oxygen exceeds the supply. Glucose-avid tumors generate lactate despite adequate oxygen tension, known as the Warburg effect. The reputation of lactate as a detrimental waste product has been established by observing its accumulation in strained muscle, ischemic tissues, and growing tumors (47, 48). Tumors also employ elevated lactate to promote an immunosuppressive state in the tumor microenvironment. The accumulation of lactate can induce the secretion of immunosuppressive factors to inhibit the immune response of NK cells and T cell. This phenomenon may also dictate immunosuppression and immune evasion of tumors in cancer immunotherapy processes where immune cell involvement and activation are crucial in tumor clearance (49). However, our observation of heightened lactate production upon IFN-γ-activation of NO-producing tumor cells raised the question of whether lactate was a waste product. Or does lactate play an essential role in the IFN-γ signaling processes? Our experiments with the inhibition of lactate dehydrogenase and monocarboxylate transporters showed that IFN-γ-induced NO-depended augmentation of lactate production feeds into NO and ROS production processes. The IFN-γ-activated H6 cells may benefit from lactate shuttling in and out of the cells and supply metabolic intermediates through gluconeogenesis to support NO and ROS production. Ultimately, the reciprocally regulated circuitry lessens the tumoral growth. This speculation was further evidenced by using potassium lactate in IFN-γ-activated H6 cells, which increased NO production and decreased cell growth (Figure 3).

The interplay of NO, HIF-1α, and lactate in IFN-γ-activated H6 cells reducing tumor growth led us to investigate the effects of these factors in non-NO-producing tumor cells with IFN-γ: CT26 and B16F10. These tumor cell lines are commonly injected into mice, subcutaneously or orthotopically, to establish tumor growth (50, 51). Our investigations revealed that CT26 cells basally express higher MHC class 1 and grow faster compared to B16F10 cells. B16F10 cells were more robust producers of lactate than CT26 cells. IFN-γ-activation of CT26 cells did not increase MHC class 1 expression as robustly as B16F10 cells. Hence, B16F10 cells displayed more inducibility with IFN-γ activation, thereby increasing the response window compared to CT26 cells. This may be the reason why IFN-γ-activated B16F10 cells exhibited significant growth reduction when intracellular HIF-1α was pharmacologically stabilized. However, potassium lactate led to significant growth reduction upon IFN-γ-activation of both non-NO-producing cell lines, CT26 and B16F10 cells (Figures 7, S8, 9).

The implications of our findings will be discussed with respect to cancer immunotherapy. Despite considerable efforts, cancer immunotherapy shows limited success with immune checkpoint blockade, only ~20.2% of patients achieved an objective response, and only ~13% achieved multiyear durable responses (52). IFN-γ can have both pro-tumorigenic and anti-tumorigenic effects by influencing all stages of tumor immunoediting. At the early growth stage, IFN-γ eliminates the tumors by increasing the expression of MHC class 1, costimulatory molecules, the immunoproteasome, antigen processing and presentation, and reducing proliferation. However, sometimes poorly immunogenic and immunoevasive transformed cells establish equilibrium and escape immune-mediated killing to progress into cancer formation (53). Patients with tumors that exhibit an active IFN-γ signature are more likely to respond favorably to immune checkpoint blockade (21, 22). Similarly, IFN-γ can modulate the expression of immunomodulatory molecules on tumor cells, making them more susceptible to CAR-T cell-mediated killing (20).

In conclusion, studying IFN-γ-driven immunometabolism is crucial for advancing cancer immunotherapy. Metabolic signatures associated with IFN-γ-driven tumor cell activation and function could serve as valuable indicators of immunotherapy efficacy. Our research enlightened the metabolic regulation of NO-producing H6 cells upon IFN-γ-activation. The IFN-γ-induced NO and ROS were important in elevating glycolytic flux and lactate production, possibly through HIF-1α stabilization. The HIF-1α function and glycolytic flux augmentation reciprocally regulated the NO and ROS production, strengthening the IFN-γ-activation signaling to induce nitrosative and oxidative stress and finally reducing tumor growth (Figure 8). Identifying patients more likely to respond to immunotherapy based on their responsiveness to IFN-γ, NO production and metabolic profiles can optimize treatment selection and minimize unnecessary exposure to ineffective therapies. Ultimately, we showed how non-NO-producing tumor cells upon IFN-γ-activation underwent cell growth reduction upon metabolic rewiring by potassium lactate. Therefore, our study shows that metabolic interventions like lactate or its analogs could make tumors more vulnerable to cancer immunotherapy. Further research is required to understand the tumor-immune interactions in detail upon IFN-γ activation and *in vivo* effects of metabolic tinkering to sensitize tumors against cancer immunotherapy.

Conclusions

Investigating the glycolytic augmentation of IFN-γ-activated H6 cells provided essential information on the mechanism of tumoral nitrosative and oxidative signaling in reducing tumor growth. Overall, the major driving factors identified here: NO, HIF-1α, and lactate, played a significant role in IFN-γ-signaling-induced tumor growth reduction. Furthermore, incorporating these driving factors, especially potassium lactate

10.3389/fimmu.2023.1282653

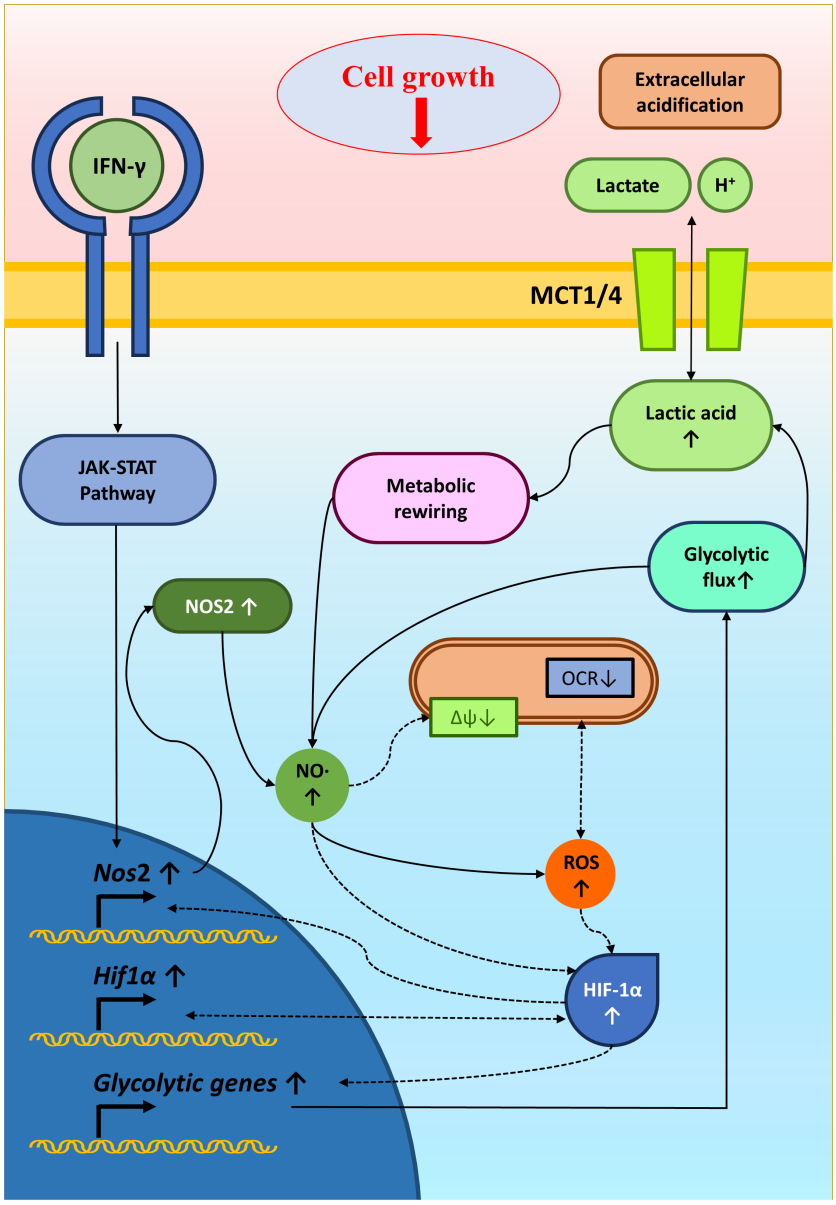

FIGURE 8
A graphical illustration of IFN-γ-mediated enhanced NO and ROS increasing glycolysis and reducing tumor growth. IFN-γ-activation of H6 cells induced NO production and NO-mediated ROS generation. NO and ROS impair mitochondrial membrane potential and may reduce mitochondrial O_2 consumption. NO, ROS and damaged mitochondrial function might stabilize HIF-1α levels. HIF-1α enhanced the glycolytic flux upon IFN-γ-activation, possibly through increasing glycolytic gene expression. The enhanced glycolytic flux increased extracellular acidification and lactate accumulation. Furthermore, the heightened glycolysis and lactate reciprocally promoted the IFN-γ-induced NO and ROS production, reducing tumor cell growth. Solid arrows indicate connections with evidence. Dashed arrows indicate probable regulations.

in non-NO-producing tumor cells to reduce tumor growth, was paramount in showing the importance of reprogrammed glycolytic metabolism in IFN-γ-signaling. These studies reinforce the roles of metabolic interventions, which may improve cancer immunotherapy outcomes.

Data availability statement

The original contributions presented in the study are included in the article/Supplementary Files, further inquiries can be directed to the corresponding author/s.

Ethics statement

Ethical approval was not required for the studies on animals in accordance with the local legislation and institutional requirements because only commercially available established cell lines were used.

Author contributions

AC: Conceptualization, Data curation, Formal Analysis, Investigation, Methodology, Validation, Writing – original draft, Writing – review & editing. SJ: Methodology, Writing – review & editing. AK: Methodology, Visualization, Writing – review & editing. NR: Methodology, Writing – review & editing. AZ: Methodology, Writing – review & editing. DN: Conceptualization, Funding acquisition, Project administration, Resources, Supervision, Visualization, Writing – review & editing.

Funding

The author(s) declare financial support was received for the research, authorship, and/or publication of this article. This study was funded by SERB grant CRG/2021/004284, core grants from IISc and the DBT-IISc partnership program. In addition, we thank the DST-FIST grant to the Department of Biochemistry, IISc for the infrastructural support.

Acknowledgments

The support of the Divisional flow facility, IISc is greatly appreciated. We thank all past and current members of the DpN laboratory for their enthusiasm in this project.

Conflict of interest

The authors declare that the research was conducted in the absence of any commercial or financial relationships that could be construed as a potential conflict of interest.

Publisher's note

Supplementary material

The Supplementary Material for this article can be found online at: https://www.frontiersin.org/articles/10.3389/fimmu.2023.1282653/full#supplementary-material

References

1. Ivashkiv LB. IFNγ: signalling, epigenetics and roles in immunity, metabolism, disease and cancer immunotherapy. *Nat Rev Immunol* (2018) 18:545–58. doi: 10.1038/s41577-018-0029-z

2. Dorman SE, Uzel G, Roesler J, Bradley JS, Bastian J, Billman G, et al. Viral infections in interferon-γ receptor deficiency. *J Pediatr* (1999) 135:640–3. doi: 10.1016/S0022-3476(99)70064-8

3. Remus N, Reichenbach J, Picard C, Rietschel C, Wood P, Lammas D, et al. Impaired interferon gamma-mediated immunity and susceptibility to mycobacterial infection in childhood. *Pediatr Res* (2001) 50:8–13. doi: 10.1203/00006450-200107000-00005

4. Ong RYL, Chan S-WB, Chew SJ, Liew WK, Thoon KC, Chong C-Y, et al. Disseminated Bacillus-Calmette-Guérin infections and primary immunodeficiency disorders in Singapore: a single center 15-year retrospective review. *Int J Infect Dis* (2020) 97:117–25. doi: 10.1016/j.ijid.2020.05.117

5. Kak G, Raza M, Tiwari BK. Interferon-gamma (IFN-γ): Exploring its implications in infectious diseases. *Biomol Concepts* (2018) 9:64–79. doi: 10.1515/bmc-2018-0007

6. Rafa H, Amri M, Saoula H, Belkhelfa M, Medjeber O, Boutaleb A, et al. Involvement of interferon-γ in bowel disease pathogenesis by nitric oxide pathway: a study in Algerian patients. *J Interferon Cytokine Res* (2010) 30:691–7. doi: 10.1089/jir.2010.0012

7. Arellano G, Ottum PA, Reyes LI, Burgos PI, Naves R. Stage-specific role of interferon-gamma in experimental autoimmune encephalomyelitis and multiple sclerosis. *Front Immunol* (2015) 6:492. doi: 10.3389/fimmu.2015.00492

8. Benchabane S, Boudjelida A, Toumi R, Belguendouz H, Youinou P, Touil-Boukoffa C. A case for IL-6, IL-17A, and nitric oxide in the pathophysiology of Sjögren's syndrome. *Int J Immunopathol Pharmacol* (2016) 29:386–97. doi: 10.1177/0394632016651273

9. Dey P, Panga V, Raghunathan S. A cytokine signalling network for the regulation of inducible nitric oxide synthase expression in rheumatoid arthritis. *PloS One* (2016) 11:e0161306. doi: 10.1371/journal.pone.0161306

10. Liu W, Zhang S, Wang J. IFN-γ, should not be ignored in SLE. *Front Immunol* (2022) 13:954706. doi: 10.3389/fimmu.2022.954706

11. Blanchette J, Jaramillo M, Olivier M. Signalling events involved in interferon-γ-inducible macrophage nitric oxide generation. *Immunology* (2003) 108:513–22. doi: 10.1046/j.1365-2567.2003.01620.x

12. Saha B, Prasanna SJ, Chandrasekar B, Nandi D. Gene modulation and immunoregulatory roles of Interferonγ. *Cytokine* (2010) 50:1–14. doi: 10.1016/j.cyto.2009.11.021

13. Martin E, Nathan C, Xie QW. Role of interferon regulatory factor 1 in induction of nitric oxide synthase. *J Exp Med* (1994) 180:977–84. doi: 10.1084/jem.180.3.977

14. Förstermann U, Sessa WC. Nitric oxide synthases: regulation and function. *Eur Heart J* (2012) 33:829–37. doi: 10.1093/eurheartj/ehr304

15. Prasanna SJ, Saha B, Nandi D. Involvement of oxidative and nitrosative stress in modulation of gene expression and functional responses by IFNγ. *Int Immunol* (2007) 19:867–79. doi: 10.1093/intimm/dxm058

16. Rakshit S, Chandrasekar BS, Saha B, Victor ES, Majumdar S, Nandi D. Interferon-gamma induced cell death: regulation and contributions of nitric oxide, cJun N-terminal kinase, reactive oxygen species and peroxynitrite. *Biochim Biophys Acta (BBA)-Molecular Cell Res* (2014) 1843:2645–61. doi: 10.1016/j.bbamcr.2014.06.014

17. Chandrasekar BS, Yadav S, Victor ES, Majumdar S, Deobagkar-Lele M, Wadhwa N, et al. Interferon-gamma and nitric oxide synthase 2 mediate the aggregation of resident adherent peritoneal exudate cells: implications for the host response to pathogens. *PloS One* (2015) 10:e0128301. doi: 10.1371/journal.pone.0128301

18. Jorgovanovic D, Song M, Wang L, Zhang Y. Roles of IFN-γ in tumor progression and regression: a review. *biomark Res* (2020) 8:1–16. doi: 10.1186/s40364-020-00228-x

19. Miller CHT, Maher SG, Young HA. Clinical use of interferon-γ. *Ann N Y Acad Sci* (2009) 1182:69–79. doi: 10.1111/j.1749-6632.2009.05069.x

20. Larson RC, Kann MC, Bailey SR, Haradhvala NJ, Llopis PM, Bouffard AA, et al. CAR T cell killing requires the IFNγR pathway in solid but not liquid tumours. *Nature* (2022) 604:563–70. doi: 10.1038/s41586-022-04585-5

21. Ayers M, Lunceford J, Nebozhyn M, Murphy E, Loboda A, Kaufman DR, et al. IFN-γ–related mRNA profile predicts clinical response to PD-1 blockade. *J Clin Invest* (2017) 127:2930–40. doi: 10.1172/JCI91190

22. Grasso CS, Tsoi J, Onyshchenko M, Abril-Rodriguez G, Ross-Macdonald P, Wind-Rotolo M, et al. Conserved interferon-γ signaling drives clinical response to immune checkpoint blockade therapy in melanoma. *Cancer Cell* (2020) 38:500–15. doi: 10.1016/j.ccell.2020.08.005

23. Siska PJ, Rathmell JC. Metabolic signaling drives IFN-γ. *Cell Metab* (2016) 24:651–2. doi: 10.1016/j.cmet.2016.10.018

24. Mah AY, Cooper MA. Metabolic regulation of natural killer cell IFN-γ production. *Crit Rev Immunol* (2016) 36:131–47. doi: 10.1615/CritRevImmunol.2016017387

25. Wang F, Zhang S, Jeon R, Vuckovic I, Jiang X, Lerman A, et al. Interferon gamma induces reversible metabolic reprogramming of M1 macrophages to sustain cell viability and pro-inflammatory activity. *EBioMedicine* (2018) 30:303–16. doi: 10.1016/j.ebiom.2018.02.009

26. Braverman J, Sogi KM, Benjamin D, Nomura DK, Stanley SA. HIF-1α is an essential mediator of IFN-γ–dependent immunity to Mycobacterium tuberculosis. *J Immunol* (2016) 197:1287–97. doi: 10.4049/jimmunol.1600266

27. Chattopadhyay A, Joseph JP, Jagdish S, Chaudhuri S, Ramteke NS, Karhale AK, et al. High throughput screening identifies auranofin and pentamidine as potent compounds that lower IFN-γ-induced Nitric Oxide and inflammatory responses in mice: DSS-induced colitis and Salmonella Typhimurium-induced sepsis. *Int Immunopharmacol* (2023) 122:110569. doi: 10.1016/j.intimp.2023.110569

28. Malu S, Srinivasan S, Maiti PK, Rajagopal D, John B, Nandi D. IFN-γ bioassay: development of a sensitive method by measuring nitric oxide production by peritoneal exudate cells from C57BL/6 mice. *J Immunol Methods* (2003) 272:55–65. doi: 10.1016/S0022-1759(02)00424-6

29. Dong S, Alahari SK. FACS-based glucose uptake assay of mouse embryonic fibroblasts and breast cancer cells using 2-NBDG probe. *Bio Protoc* (2018) 8:e2816–6. doi: 10.21769/BioProtoc.2816

30. Crowley LC, Christensen ME, Waterhouse NJ. Measuring mitochondrial transmembrane potential by TMRE staining. *Cold Spring Harb Protoc* (2016) 2016. doi: 10.1101/pdb.prot087361

31. Mahmood T, Yang P-C. Western blot: technique, theory, and trouble shooting. *N Am J Med Sci* (2012) 4:429. doi: 10.4103/1947-2714.100998

32. Mookerjee SA, Brand MD. Measurement and analysis of extracellular acid production to determine glycolytic rate. *JoVE (Journal Visualized Experiments)* (2015) 106:e53464. doi: 10.3791/53464

33. Hopkins E, Sanvictores T, Sharma S. Physiology, acid base balance. In: *StatPearls [Internet]*. Treasure Island (FL): StatPearls Publishing (2022).

34. Payne CM, Bernstein H, Bernstein C, Kunke K, Garewal H. The specific NOS2 inhibitor, 1400W, sensitizes HepG2 cells to genotoxic, oxidative, xenobiotic, and endoplasmic reticulum stresses. *Antioxid Redox Signal* (2001) 3:931–6. doi: 10.1089/15230860152665082

35. Nakaki T, Hishikawa K. The arginine paradox. *Nihon Yakurigaku Zasshi* (2002) 119:7–14. doi: 10.1254/fpj.119.7

36. Li D-Y, Gao S-J, Sun J, Zhang L-Q, Wu J-Y, Song F-H, et al. Targeting the nitric oxide/cGMP signaling pathway to treat chronic pain. *Neural Regener Res* (2023) 18:996–1003. doi: 10.4103/1673-5374.355748

37. Raychaudhuri D, Bhattacharya R, Sinha BP, Liu CSC, Ghosh AR, Rahaman O, et al. Lactate induces pro-tumor reprogramming in intratumoral plasmacytoid dendritic cells. *Front Immunol* (2019) 10:1878. doi: 10.3389/fimmu.2019.01878

38. Lum JJ, Bui T, Gruber M, Gordan JD, DeBerardinis RJ, Covello KL, et al. The transcription factor HIF-1α plays a critical role in the growth factor-dependent regulation of both aerobic and anaerobic glycolysis. *Genes Dev* (2007) 21:1037–49. doi: 10.1101/gad.1529107

39. Downes NL, Laham-Karam N, Kaikkonen MU, Ylä-Herttuala S. Differential but complementary HIF1α and HIF2α transcriptional regulation. *Mol Ther* (2018) 26:1735–45. doi: 10.1016/j.ymthe.2018.05.004

40. Mishra D, Banerjee D. Lactate dehydrogenases as metabolic links between tumor and stroma in the tumor microenvironment. *Cancers (Basel)* (2019) 11:750. doi: 10.3390/cancers11060750

41. Davies EA, Saleh C, Bannard-Smith J. Recovery from profound acidosis (pH 6.685) in multi-organ dysfunction syndrome. *J Intensive Care Soc* (2021) 22:78–82. doi: 10.1177/1751143719870102

42. Rizi BS, Achreja A, Nagrath D. Nitric oxide: the forgotten child of tumor metabolism. *Trends Cancer* (2017) 3:659–72. doi: 10.1016/j.trecan.2017.07.005

43. Tengan CH, Moraes CT. NO control of mitochondrial function in normal and transformed cells. *Biochim Biophys Acta (BBA)-Bioenergetics* (2017) 1858:573–81. doi: 10.1016/j.bbabio.2017.02.009

44. Masoud GN, Li W. HIF-1α pathway: role, regulation and intervention for cancer therapy. *Acta Pharm Sin B* (2015) 5:378–89. doi: 10.1016/j.apsb.2015.05.007

45. Dehne N, Brüne B. Sensors, transmitters, and targets in mitochondrial oxygen shortage—a hypoxia-inducible factor relay story. *Antioxid Redox Signal* (2014) 20:339–52. doi: 10.1089/ars.2012.4776

46. Parra-Izquierdo I, Castaños-Mollor I, López J, Gómez C, San Román JA, Crespo MS, et al. Lipopolysaccharide and interferon-γ team up to activate HIF-1α via STAT1 in normoxia and exhibit sex differences in human aortic valve interstitial cells. *Biochim Biophys Acta (BBA)-Molecular Basis Dis* (2019) 1865:2168–79. doi: 10.1016/j.bbadis.2019.04.014

47. Rabinowitz JD, Enerbäck S. Lactate: the ugly duckling of energy metabolism. *Nat Metab* (2020) 2:566–71. doi: 10.1038/s42255-020-0243-4

48. Goodwin ML, Gladden LB, Nijsten MWN, Jones KB. Lactate and cancer: revisiting the Warburg effect in an era of lactate shuttling. *Front Nutr* (2015) 1:27. doi: 10.3389/fnut.2014.00027

49. Zhang Y, Zhang Z. The history and advances in cancer immunotherapy: understanding the characteristics of tumor-infiltrating immune cells and their therapeutic implications. *Cell Mol Immunol* (2020) 17:807–21. doi: 10.1038/s41423-020-0488-6

50. Barrera-Avalos C, Díaz X, Madrid B, Michelson SA, Robles-Planells C, Sánchez-Guerrero G, et al. *In vivo* antitumor effect against murine cells of CT26 colon cancer and EL4 lymphoma by autologous whole tumor dead cells. *BioMed Res Int* (2021) 2021:1–16. doi: 10.1155/2021/6626851

51. Yokomizo K, Waki K, Ozawa M, Yamamoto K, Ogasawara S, Yano H, et al. Knockout of high-mobility group box 1 in B16F10 melanoma cells induced host immunity-mediated suppression of *in vivo* tumor growth. *Med Oncol* (2022) 39:58. doi: 10.1007/s12032-022-01659-2

52. Revisiting checkpoint blockade. *Nat Biotechnol* (2022) 40:981. doi: 10.1038/s41587-022-01407-x

53. Alspach E, Lussier DM, Schreiber RD. Interferon γ and its important roles in promoting and inhibiting spontaneous and therapeutic cancer immunity. *Cold Spring Harb Perspect Biol* (2019) 11:a028480. doi: 10.1101/cshperspect.a028480